Dislocation-induced acoustic nonlinearity parameter in crystalline solids

Zimu Chen and Jianmin Qu

Citation: Journal of Applied Physics **114**, 164906 (2013); doi: 10.1063/1.4826523
View online: http://dx.doi.org/10.1063/1.4826523
View Table of Contents: http://scitation.aip.org/content/aip/journal/jap/114/16?ver=pdfcov
Published by the AIP Publishing

Dislocation-induced acoustic nonlinearity parameter in crystalline solids

Zimu Chen[1] and Jianmin Qu[2,3,a)]
[1]*School of Materials Science and Engineering, Beihang University, Beijing 100191, People's Republic of China*
[2]*Department of Civil and Environmental Engineering, Northwestern University, Evanston, Illinois 60208, USA*
[3]*Department of Mechanical Engineering, Northwestern University, Evanston, Illinois 60208, USA*

(Received 8 July 2013; accepted 6 October 2013; published online 28 October 2013)

Based on an orientation-dependent dislocation line energy, a solution to the acoustic nonlinearity parameter is obtained for pure and mixed dislocations in anisotropic crystals. The solution is validated by comparison with molecular dynamic simulations. Parametric studies using this new solution show that (i) elastic anisotropy can significantly change the nonlinear behavior of dislocations including "corners" in the bowed dislocation line, much reduced critical stress for instability, sharp peaks in the β versus applied shear relationship, etc., (ii) mixed dislocations may have distinct behavior that is not bounded by the pure edge and screw dislocations, (iii) asymptotic solutions of the acoustic nonlinearity parameter in terms of power series (as high as 5th order) may not be valid even for pure dislocations in isotropic solids. © *2013 AIP Publishing LLC*.
[http://dx.doi.org/10.1063/1.4826523]

I. INTRODUCTION

When a monochromic longitudinal wave propagates through an elastic solid with quadratic nonlinearity, higher order harmonic waves are generated. Amplitude of the second order harmonic wave depends on the second and third order elastic constants (TOE), as well as material defects such as dislocations. Since the density of dislocations is usually correlated with fatigue damage in metallic materials, the amplitude of the second order harmonic wave can be used as a measure of fatigue damage. This approach has been used extensively[1–4] to assess fatigue damage nondestructively in metallic materials.

In a perfect single crystal with quadratic elastic nonlinearity, the first Piola-Kirchhoff stress tensor is related to the displacement gradients through[5]

$$\sigma_{ij} = A_{ijkl}u_{k,l} + \frac{1}{2}A_{ijklmn}u_{k,l}u_{m,n}, \tag{1}$$

where A_{ijkl} and A_{ijklmn} are, respectively, the second and third order Huang coefficients. It can be easily shown that, for a one-dimensional wave of polarization d_i propagating in the p_i direction, the amplitude of the second order harmonic wave is controlled by the acoustic nonlinearity parameter attributed to lattice anharmonicity[6]

$$\beta^l = \frac{A_{ijklmn}p_jp_lp_nd_id_kd_m}{A_{ijkl}p_jp_ld_id_k}. \tag{2}$$

When dislocations are present in the crystal, additional acoustic nonlinearity is introduced. By assuming elastic isotropy and constant (orientation independent) dislocation line tension, Hikata *et al.*[7] and Cantrell[6] derived

$$\beta = \beta^l + \beta^d, \tag{3}$$

where

$$\beta^d = \frac{24\Omega R^3}{5}(\Lambda b^2)\left(\frac{L}{b}\right)^4\left(\frac{\sigma}{\mu}\right), \tag{4}$$

is due to the presence of dislocations with Λ being the dislocation density, L the dislocation length, b the length of the Burgers vector, σ the applied stress, μ the shear modulus, R an orientation factor between the applied stress and the resolved shear stress, and Ω the conversion factor between the shear strain in the slip direction and measured strain. According to this model, the dislocation induced β^d should increase linearly with the applied stress σ. However, this does not agree with a number of experimental measurements including some of the data presented in Hikata's original paper.[7]

Since β^d has been used extensively in recent years to monitor fatigue damage, it is critically important that correct models are developed to correlate β^d with material defects. Recently, Cash and Cai[8] developed a new model using an orientation-dependent dislocation line energy for the cases of initially pure edge and screw dislocations in isotropic materials. By isotropic materials, we mean materials whose elastic response is independent of the materials' orientation. For cubic crystals, elastic isotropy means their elastic constants satisfy $C_{11} - C_{12} = 2C_{44}$. By solving an implicit equation, these authors demonstrated that the original model by Hikata *et al.*[7] based on a constant line energy assumption fails to capture the correct behavior of β^d for edge dislocations in materials with a Poisson's ratio greater than 0.2.

In this study, a different approach is taken to develop a new model that is applicable to anisotropic crystals, and capable of dealing with mixed dislocations. As a by-product, the newly developed model yields the exact and explicit solutions to pure dislocations in isotropic materials. Our model predictions show that (i) elastic anisotropy can significantly change the nonlinear behavior of dislocations including

a)Electronic mail: j-qu@northwestern.edu

"corners" in the bowed dislocation line, much reduced critical stress for instability, sharp peaks in the β versus applied shear relationship, etc., (ii) mixed dislocations may have distinct behavior that is not bounded by the pure edge and screw dislocations, (iii) asymptotic solutions of the acoustic nonlinearity parameter in terms of power series (as high as 5th order) may not be valid even for pure dislocations in isotropic solids.

The paper is arranged as follows. By taking advantages of the coordinate-free nature of the Barnett-Lothe tensors,[9] Sec. II develops the exact solution to the dislocation line energy in anisotropic solids. The equations to determine the equilibrium bow out shape of mixed dislocations under a given shear stress is developed and solved in Sec. III. Section IV solves for the shear strain induced by dislocation bowing out. In Sec. V, molecular dynamic (MD) simulations are conducted to validate the continuum models developed in Secs. II–IV. Section VI investigates the critical shear stress that causes unstable dislocation bowing, or the onset of Frank-Read source. The acoustic nonlinearity parameter β^d is derived in Sec. VII based on the solutions derived in Sec. IV for the dislocation induced shear strains. Section VIII discusses the dependence of β^d on the dislocation segment length. Summary and conclusions are presented in Sec. IX.

II. LINE ENERGY OF A STRAIGHT DISLOCATION IN ANISOTROPIC SOLIDS

Consider a straight dislocation in a large single crystal with elastic stiffness tensor given by $\mathbf{C} = C_{ijkl}\mathbf{e}_i^c\mathbf{e}_j^c\mathbf{e}_k^c\mathbf{e}_l^c$, where $\{\mathbf{e}_1^c, \mathbf{e}_2^c, \mathbf{e}_3^c\}$ is a triad of mutually orthogonal unit vectors that are aligned with the crystallographic orientations of the single crystal, and C_{ijkl} are the corresponding elastic constants, Fig. 1. The dislocation is described by the unit vector $\mathbf{t} = t_i\mathbf{e}_i^c$ representing the direction of the dislocation line, the unit normal $\mathbf{s} = s_i\mathbf{e}_i^c$ of the slip plane, and the Burgers vector $\mathbf{b} = b\hat{\mathbf{b}}$ with $\hat{\mathbf{b}} = \hat{b}_i\mathbf{e}_i^c$ being a unit vector. Further, both $\hat{\mathbf{b}}$ and $\mathbf{t}$ are orthogonal to $\mathbf{s}$, i.e., $\mathbf{s}\cdot\mathbf{t} = \mathbf{s}\cdot\hat{\mathbf{b}} = 0$ which means that $\mathbf{t}$ and $\hat{\mathbf{b}}$ are both within the slip plane. Without loss of generality, we introduce a Cartesian coordinate system by another triad of mutually orthogonal unit vectors $\{\mathbf{e}_1, \mathbf{e}_2, \mathbf{e}_3\}$ that are aligned with the dislocation so that $\mathbf{e}_1 = \hat{\mathbf{b}}$, $\mathbf{e}_3 = \mathbf{s}$, and $\mathbf{e}_2 = \mathbf{e}_3 \times \mathbf{e}_1 = \mathbf{s} \times \hat{\mathbf{b}} = \varepsilon_{pqi}s_p\hat{b}_q\mathbf{e}_i^c$, where ε_{ijk} is the permutation symbol.

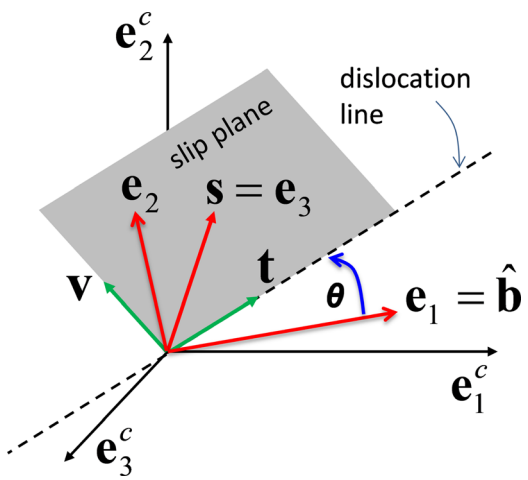

FIG. 1. A straight dislocation in the direction of $\mathbf{t}$ with Burgers vector $\mathbf{b}$.

Next, we use θ to denote the angle between $\hat{\mathbf{b}}$ and $\mathbf{t}$, i.e., $\mathbf{t}\cdot\hat{\mathbf{b}} = \cos\theta$. It then follows that

$$\mathbf{t} = t_i\mathbf{e}_i^c = \cos\theta\mathbf{e}_1 + \sin\theta\mathbf{e}_2 = \cos\theta\hat{\mathbf{b}} + \sin\theta\mathbf{s}\times\hat{\mathbf{b}} = (\cos\theta\hat{b}_i + \sin\theta\varepsilon_{pqi}s_p\hat{b}_q)\mathbf{e}_i^c. \quad (5)$$

In other words, $\mathbf{t}$ can be written in terms of $\mathbf{s}$, $\hat{\mathbf{b}}$, and θ. For future reference, we introduce another unit vector

$$\mathbf{v} = \mathbf{s}\times\mathbf{t} = \mathbf{s}\times(\cos\theta\hat{\mathbf{b}} + \sin\theta\mathbf{s}\times\hat{\mathbf{b}}) = \cos\theta\mathbf{s}\times\hat{\mathbf{b}} - \sin\theta\hat{\mathbf{b}} = (\cos\theta\varepsilon_{pqi}s_p\hat{b}_q - \sin\theta\hat{b}_i)\mathbf{e}_i^c, \quad (6)$$

so that $\{\mathbf{t}, \mathbf{v}, \mathbf{s}\}$ forms another triad of three mutually orthogonal unit vectors.

It is well known[9] that the line energy of such a dislocation is given by

$$E(\theta) = E_0K(\theta), \quad (7)$$

where $E_0 = (C_{44}b^2/4\pi)\ln(R_0/r_0)$ is the line energy of a screw dislocation in an isotropic solid with shear modulus C_{44}, with R_0 being the dimension of the crystal, and r_0 the radius of the dislocation core. We note that E_0 has the dimension of force. It has been suggested that $\ln(R_0/r_0) \approx 2\pi$ by many authors, e.g., Hikata *et al.*[7] and Cash and Cai[8] so that $E_0 = C_{44}b^2/2$. The $K(\theta)$ in Eq. (7) is the (dimensionless) pre-logarithmic factor that accounts for the mixed (edge and screw) nature of the dislocation and the elastic anisotropy. It is a function of the elastic constants of the crystal and the dislocation's orientation with respect to the crystal axes,[9–11] i.e.,

$$K(\theta) = \frac{1}{C_{44}}\hat{\mathbf{b}}^T\mathbf{L}(\theta)\hat{\mathbf{b}}, \quad (8)$$

where

$$\mathbf{L}(\theta) = L_{ij}(\theta)\mathbf{e}_i^c\mathbf{e}_j^c = -\frac{1}{\pi}\int_0^\pi \mathbf{N}(\theta,\omega)d\omega \quad (9)$$

is one of the three well-known Barnett-Lothe tensors in anisotropic elasticity.[9] The integrand is given by

$$\mathbf{N}(\theta,\omega) = \mathbf{R}\mathbf{T}^{-1}\mathbf{R}^T - \mathbf{Q}, \quad (10)$$

with

$$Q_{ij} = C_{pijq}m_pm_q, \quad R_{ij} = C_{pijq}m_pn_q, \quad T_{ij} = C_{pijq}n_pn_q, \quad (11)$$

where $\mathbf{m}$ and $\mathbf{n}$ are unit vectors defined by, Fig. 2,

$$\mathbf{m} = \cos\omega\mathbf{v} + \sin\omega\mathbf{s}, \quad \mathbf{n} = -\sin\omega\mathbf{v} + \cos\omega\mathbf{s}. \quad (12)$$

It then follows from Eq. (6) that

$$\mathbf{m} = (\cos\theta\mathbf{s}\times\hat{\mathbf{b}} - \sin\theta\hat{\mathbf{b}})\cos\omega + \sin\omega\mathbf{s} = [(\cos\theta\varepsilon_{pqi}s_p\hat{b}_q - \sin\theta\hat{b}_i)\cos\omega + \sin\omega s_i]\mathbf{e}_i^c, \quad (13)$$

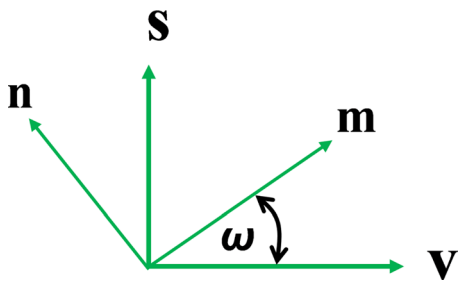

FIG. 2. Definition of **m** and **n**.

$$\mathbf{n} = -(\cos\theta \mathbf{s} \times \hat{\mathbf{b}} - \sin\theta \hat{\mathbf{b}})\sin\omega + \cos\omega \mathbf{s}$$
$$= [-(\cos\theta \varepsilon_{pqi} s_p \hat{b}_q - \sin\theta \hat{b}_i)\sin\omega + \cos\omega s_i]\mathbf{e}_i^c. \quad (14)$$

If **m** and **n** are considered functions of θ and ω, one can easily see that

$$\mathbf{m}(\theta+\pi, \pi-\omega) = \mathbf{m}(\theta,\omega), \quad \mathbf{n}(\theta+\pi,\pi-\omega) = -\mathbf{n}(\theta,\omega). \quad (15)$$

Thus, $\mathbf{N}(\theta+\pi,\pi-\omega) = \mathbf{N}(\theta,\omega)$. Finally,

$$\mathbf{L}(\theta) = -\frac{1}{\pi}\int_0^\pi \mathbf{N}(\theta,\omega)d\omega$$
$$= -\frac{1}{\pi}\int_0^\pi \mathbf{N}(\theta+\pi,\pi-\omega)d\omega$$
$$= \mathbf{L}(\theta+\pi), \quad (16)$$

which means that $K(\theta+\pi) = K(\theta)$. Along the same line, one can easily show that such a periodicity also holds for any derivatives of $K(\theta)$, i.e., $K^{(n)}(\theta+\pi) = K^{(n)}(\theta)$. These results can also be argued by symmetry. Changing θ to $\theta+\pi$ merely reverses the direction of the dislocation line, which physically corresponds to the same dislocation.

In closing this section, we note that in evaluating the $K(\theta)$ above, the elastic constants used are their values in the crystallographic coordinate system, regardless the orientations of the dislocation and its Burgers vector. This tremendous advantage is made possible by the coordinate-free nature of the Barnett-Lothe tensors.[9]

III. EQUILIBRIUM SHAPE OF A PINNED DISLOCATION SUBJECT TO AN APPLIED SHEAR STRESS

Consider a dislocation segment of length L, pinned at both ends, subjected to a shear stress field within the slip plane. For convenience, x_i will be used to denote the coordinates of an arbitrary field location in the Cartesian coordinate system defined by the triad $\{\mathbf{e}_1, \mathbf{e}_2, \mathbf{e}_3\}$ introduced in the previous section. Without loss of generality, one may assume that the dislocation segment lies along the line $x_2 = x_1 \tan\theta_0$, when no external stress is applied. The pinning points are at (0, 0, 0) and $(L\cos\theta_0, L\sin\theta_0, 0)$, respectively, Fig. 3.

When the shear stress σ_{13} is applied, the dislocation segment may bow out in the slip plane. The equilibrium shape of the bowed dislocation segment is given by[12]

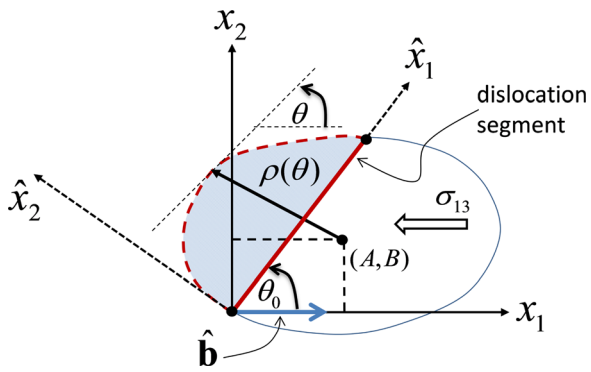

FIG. 3. A dislocation segment pinned at both ends subjected to a shear stress.

$$x_1 - AL = \frac{L}{\kappa}X(\theta), \quad x_2 - BL = \frac{L}{\kappa}Y(\theta), \quad \text{for } 0 \le \theta < 2\pi, \quad (17)$$

where $\kappa = \sigma_{13} bL/E_0$ is a dimensionless number that is proportional to the applied shear stress and the dislocation length L, θ is the angle between the tangential direction of the bowed dislocation line and the x_1-axis, and (A, B) is the center of the closed contour

$$\rho^2(\theta) = \left(\frac{x_1}{L} - A\right)^2 + \left(\frac{x_2}{L} - B\right)^2$$
$$= \frac{1}{\kappa^2}(X^2(\theta) + Y^2(\theta))$$
$$= \frac{1}{\kappa^2}(K^2(\theta) + [K'(\theta)]^2). \quad (18)$$

Clearly, κ represents the driving force for the dislocation bowing, i.e., large κ leads to more bowing. The dimensionless angular functions are defined by

$$X(\theta) = -K(\theta)\sin\theta - K'(\theta)\cos\theta,$$
$$Y(\theta) = K(\theta)\cos\theta - K'(\theta)\sin\theta. \quad (19)$$

The constants A and B in Eq. (17) can be determined by the conditions at the pinning points

$$0 - A = \frac{X(\theta_1)}{\kappa}, \quad 0 - B = \frac{Y(\theta_1)}{\kappa}, \quad (20)$$

$$\cos\theta_0 - A = \frac{X(\theta_2)}{\kappa}, \quad \sin\theta_0 - B = \frac{Y(\theta_2)}{\kappa}, \quad (21)$$

where θ_1 and θ_2 are the values of θ at the pinning points (0, 0) and $(L\cos\theta_0, L\sin\theta_0)$, respectively. Eliminating A and B yields,

$$X(\theta_2) - X(\theta_1) = \kappa\cos\theta_0, \quad Y(\theta_2) - Y(\theta_1) = \kappa\sin\theta_0. \quad (22)$$

This is a pair of nonlinear algebraic equations for the two unknowns θ_1 and θ_2. Numerical methods are typically needed for the solution. Once θ_1 and θ_2 are solved, the constants A and B can be evaluated from Eq. (20). We note that the dependence of θ_1 and θ_2 on the dislocation segment length L comes through their dependence on κ. In other

words, θ_1 and θ_2 do no change with changing L unless κ changes.

In this paper, we limit ourselves to the case where the line tension is positive over the entire dislocation segment, i.e.,

$$T(\theta) = K(\theta) + K''(\theta) > 0 \quad \text{for all } \theta. \tag{23}$$

This condition ensures that the curve described by Eq. (18) is a singly connected closed contour in the x_1x_2-plane without kinks.[12,13]

IV. SHEAR STRAIN DUE TO DISLOCATION BOW OUT

The shear strain due to dislocation bowing out can be written as[6,7]

$$\varepsilon_{13}^{dis} = \frac{\Lambda b S}{L}, \tag{24}$$

where Λ is the dislocation density (length/volume), S is the area swept by the dislocation bowing, see the shaded area in Fig. 3, which can be calculated by

$$S = \int_0^L \hat{x}_2 d\hat{x}_1 = \int_{\theta_1}^{\theta_2} \hat{x}_2(\theta)\hat{x}_1'(\theta)d\theta, \tag{25}$$

where

$$\hat{x}_1 = x_1\cos\theta_0 + x_2\sin\theta_0, \quad \hat{x}_2 = -x_1\sin\theta_0 + x_2\cos\theta_0. \tag{26}$$

Making use of Eq. (17) in Eq. (25) in conjunction with Eqs. (20), (21), and (26) yields

$$\begin{aligned}\bar{S}(\kappa) \equiv \frac{S}{L^2} = \frac{1}{\kappa^2}\int_{\theta_1}^{\theta_2} &[Y(\theta)\cos\theta_0 - X(\theta)\sin\theta_0] \\ &\times [Y'(\theta)\sin\theta_0 + X'(\theta)\cos\theta_0]d\theta \\ &-\frac{1}{\kappa}[Y(\theta_1)\cos\theta_0 - X(\theta_1)\sin\theta_0].\end{aligned} \tag{27}$$

In terms of $K(\theta)$

$$\begin{aligned}\bar{S}(\kappa) = \frac{-1}{\kappa^2}\int_{\theta_1}^{\theta_2} &\cos(\theta-\theta_0)[\cos(\theta-\theta_0)K(\theta) \\ &-\sin(\theta-\theta_0)K'(\theta)][K(\theta)+K''(\theta)]d\theta \\ &-\frac{1}{\kappa}[\cos(\theta_0-\theta_1)K(\theta) + \sin(\theta_0-\theta_1)K'(\theta)].\end{aligned} \tag{28}$$

Finally, Eq. (24) can be written as

$$\varepsilon_{13}^{dis} = \Lambda b L \bar{S}(\kappa). \tag{29}$$

Again, we note that $\bar{S}(\kappa)$ is a dimensionless function of κ only. It does not depend on L explicitly.

Example 1—Isotropic materials: If the crystal is idealized as elastically isotropic, the elastic constants can be written as

$$\begin{aligned}C_{ijkl} = C_{ijkl}^0 &= \lambda\delta_{ij}\delta_{kl} + \mu(\delta_{ik}\delta_{jl} + \delta_{il}\delta_{jk}) \\ &= \mu\left(\frac{2\nu}{1-2\nu}\delta_{ij}\delta_{kl} + \delta_{ik}\delta_{jl} + \delta_{il}\delta_{jk}\right).\end{aligned} \tag{30}$$

It then follows from Eq. (11) that

$$\begin{aligned}&\frac{Q_{ij}}{\mu} = \delta_{ij} + \frac{m_i m_j}{1-2\nu}, \quad \frac{T_{ij}}{\mu} = \delta_{ij} + \frac{n_i n_j}{1-2\nu}, \\ &\frac{R_{ij}}{\mu} = \frac{2\nu}{1-2\nu}m_i n_j + m_j n_i + m_p n_p \delta_{ij}.\end{aligned} \tag{31}$$

It can be verified that

$$\begin{aligned}\mathbf{T}^{-1} = &\frac{1}{2(1-\nu)\mu} \\ &\times \begin{bmatrix} 2(1-\nu)-n_1n_1 & -n_1n_2 & -n_1n_3 \\ -n_1n_2 & 2(1-\nu)-n_2n_2 & -n_2n_3 \\ -n_1n_3 & -n_2n_3 & 2(1-\nu)-n_3n_3 \end{bmatrix}.\end{aligned} \tag{32}$$

Substituting Eqs. (31) and (32) into Eq. (8) yields

$$K(\theta) = \frac{1}{1-\nu}(1-\nu\cos^2\theta). \tag{33}$$

This is identical to the result in the existing literature.[12] It then follows from Eq. (7) that the strain energy per unit length of the dislocation is given by

$$E = \frac{Kb^2}{4\pi}\ln\left(\frac{R}{r_0}\right) = \frac{E_0}{(1-\nu)}(1-\nu\cos^2\theta). \tag{34}$$

Substituting Eq. (33) into Eq. (19) yields

$$\begin{aligned}X(\theta) &= \frac{-1}{2(1-\nu)}(2+\nu+\nu\cos 2\theta)\sin\theta, \\ Y(\theta) &= \frac{1}{2(1-\nu)}(2-3\nu+\nu\cos 2\theta)\cos\theta.\end{aligned} \tag{35}$$

Clearly, when $\nu = 0$, (35) reduces to $X(\theta) = -\sin\theta$, $Y(\theta) = \cos\theta$ which represent a unit circle. This is the case when one assumes that the dislocation line tension is a constant independent of its orientation.

Plotted in Fig. 4 is $\kappa\rho(\theta) = \sqrt{X^2(\theta)+Y^2(\theta)}$ as a function of θ. According to Eq. (17), any portion of this closed contour could be the equilibrium shape of a dislocation segment. We are interested in the portion of the contour in Fig. 4 that corresponds to the equilibrium shape of a

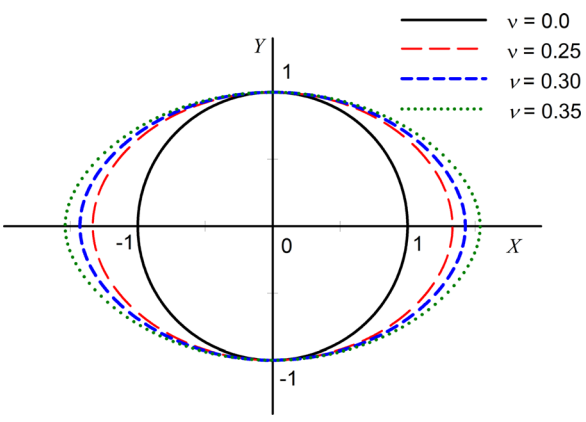

FIG. 4. Contour representing all potential equilibrium shape of a dislocation segment in isotropic solids.

dislocation of length L under a given shear stress σ_{13}. It is assumed that the initial (before σ_{13} is applied) angle between the dislocation segment and its Burgers vector (the x_1-direction) is θ_0. To this end, we make use of Eq. (35) in Eq. (22) to arrive at two transcendental equations for θ_1 and θ_2

$$(1+\nu\cos^2\theta_2)\sin\theta_2-(1+\nu\cos^2\theta_1)\sin\theta_1 = -(1-\nu)\kappa\cos\theta_0, \tag{36}$$

$$(1-2\nu+\nu\cos^2\theta_2)\cos\theta_2-(1-2\nu+\nu\cos^2\theta_1)\cos\theta_1 = (1-\nu)\kappa\sin\theta_0. \tag{37}$$

Numerical techniques are typically required to solve these equations. Once θ_1 and θ_2 are solved from the above, they can be used in Eq. (35), then in Eq. (27) to yield

$$\bar{S}=\frac{f(\theta_1,\theta_2)}{64\kappa^2(1-\nu)^2}, \tag{38}$$

where $f(\theta_1,\theta_2)$ is a known function of θ_1 and θ_2. An explicit expression of $f(\theta_1,\theta_2)$ is given in Appendix A. Therefore, once Eqs. (36) and (37) are solved, the area swept by the dislocation bowing can be easily calculated from Eq. (38).

In what follows, we will consider an initially screw dislocation, i.e., $\theta_0=0$. In this case, Eq. (37) is identically satisfied by setting $\theta_1=-\theta_2$, and Eq. (36) reduces to

$$2[1+(1-\sin^2\theta_2)\nu]\sin\theta_2+(1-\nu)\kappa=0. \tag{39}$$

For $\nu\neq 0$, Eq. (39) is a cubic equation for $\sin\theta_2$, so there will be three roots. A physically meaningful root must be real and no greater than unity. For small enough κ, the real root of Eq. (39) that is not greater than unity is

$$\sin\theta_2=z+\bar{z}, \tag{40}$$

where the over bar denotes complex conjugate, and

$$z=-\frac{(1+i\sqrt{3})\left(9\nu^2(1-\nu)\kappa+i\sqrt{3}\nu^{3/2}\sqrt{16(1+\nu)^3-27(1-\nu)^2\nu\kappa^2}\right)^{1/3}}{2\times 6^{2/3}\nu}. \tag{41}$$

One can show that $\lim_{\nu\to 0}(z+\bar{z})=-\kappa/2$, which is what one would get from Eq. (39) directly by setting $\nu=0$.

We note that when κ is large enough, no physically meaningful root exits. This means that the driving force (either stress or dislocation length) is too large to maintain a stable equilibrium shape of the bowed dislocation segment. The critical value of κ beyond which stable solution does exist will be discussed later in this paper.

Since θ_2 is known from Eq. (40), and $\theta_1=-\theta_2$, one can use Eq. (27) to calculate the area swept by the dislocation bowing

$$\bar{S}(\kappa)=\frac{4[\nu^2-8(1-\nu)]\theta_2+(16-3\nu^2-32\nu)\sin 2\theta_2+(8-\nu)\nu\sin 4\theta_2+\nu^2\sin 6\theta_2}{32(1-\nu)^2\kappa^2}. \tag{42}$$

Unlike the asymptotic solution given by Cash and Cai,[8] Eq. (42) in conjunction with Eq. (40) provides an exact solution to S. The asymptotic expression of Eq. (42) for small κ can be computed in a straightforward fashion from Eq. (42),

$$\bar{S} = s_1\frac{\sigma_{13}bL}{E_0}+s_3\left(\frac{\sigma_{13}bL}{E_0}\right)^3+s_5\left(\frac{\sigma_{13}bL}{E_0}\right)^5+\cdots=s_1\kappa+s_3\kappa^3+s_5\kappa^5+\cdots, \tag{43}$$

where

$$s_1=\frac{(1-\nu)}{12(1+\nu)},\quad s_3=\frac{(1-\nu)^3(1+3\nu)}{160(1+\nu)^4},\quad s_5=\frac{3(1-\nu)^5(1+6\nu+13\nu^2)}{3584(1+\nu)^7}. \tag{44}$$

It is easily seen that this is identical to the asymptotic solution of Cash and Cai.[8]

Next, consider an initially edge dislocation, i.e., $\theta_0=\pi/2$. In this case, one may take $\theta_1=\pi-\theta_2$, so that Eq. (36) is identically satisfied, and Eq. (37) reduces to

$$2[1-(2-\cos^2\theta_2)\nu]\cos\theta_2-(1-\nu)\kappa=0. \tag{45}$$

The physically meaningful root is

$$\cos\theta_2 = \frac{-2(1-2\nu)\nu + \left(9\kappa\nu^2(1-\nu) + \sqrt{3\nu^3[27\kappa^2(1-\nu)^2\nu + 16(1-2\nu)^3]}\right)^{2/3}}{6^{1/3}\nu\left(9\kappa\nu^2(1-\nu) + \sqrt{3\nu^3[27\kappa^2(1-\nu)^2\nu + 16(1-2\nu)^3]}\right)^{1/3}}. \tag{46}$$

The area swept by the dislocation bowing is thus

$$\bar{S}(\kappa) = \frac{2[\nu^2 - 8(1-\nu)](\pi - 2\theta_2) + (16 - 19\nu^2)\sin 2\theta_2 + (8-7\nu)\nu\sin 4\theta_2 + \nu^2\sin 6\theta_2}{32(1-\nu)^2\kappa^2}. \tag{47}$$

Again, this is an exact solution. As stated in Cash and Cai,[8] their asymptotical solution for the initially edge dislocation is appropriate only for small Poisson's ratio, $\nu < 0.25$. Our solution here, however, is valid for any $0 \le \nu < 0.5$.

Again, one may wish to obtain the leading terms in the asymptotic expression of Eq. (47) for small κ

$$\begin{aligned}\bar{S} &= s_1\frac{\sigma_{13}bL}{E_0} + s_3\left(\frac{\sigma_{13}bL}{E_0}\right)^3 + s_5\left(\frac{\sigma_{13}bL}{E_0}\right)^5 + \cdots \\ &= s_1\kappa + s_3\kappa^3 + s_5\kappa^5 + \cdots,\end{aligned} \tag{48}$$

where

$$s_1 = \frac{(1-\nu)}{12(1-2\nu)}, \quad s_3 = \frac{(1-\nu)^3(1-4\nu)}{160(1-2\nu)^4}, \quad s_5 = \frac{3(1-\nu)^5(1-8\nu+20\nu^2)}{3584(1-2\nu)^7}. \tag{49}$$

To investigate the validity of the asymptotic solutions, comparisons between the asymptotic and the exact solutions are made. Shown in Figs. 5 and 6 are the $\bar{S}(\kappa)$ versus κ curves for various values of ν, where the length of the dislocation segment is chosen so that $L/b = 2000$. Fig. 5 is for the screw dislocation. Clearly, the asymptotic solution compares very well with the exact solution for the full range of ν even for κ as large as 1.2. For the edge dislocation, Fig. 6, the asymptotic solution is close to the exact solution up to about $\kappa = 1.0$ for smaller Poisson's ratio $\nu < 0.2$. For larger ν, the asymptotic solution starts to deviate from the exact solution around $\kappa = 0.4$. Another observation is that the edge dislocation is much easier to bow than the screw dislocation because under the same shear stress, the area swept by the edge dislocation bowing is more than twice that swept by a screw dislocation. Also, as will be seen later in this paper, the critical value for κ before instability sets in is about $\kappa_c \approx 2$ for the edge dislocation and $\kappa_c \approx 2.7$ for the screw dislocation.

For mixed dislocations $0 < \theta_0 < \theta/2$, Eqs. (36) and (37) do not seem to have explicit solutions for θ_1 and θ_2. Fortunately, numerical solutions are rather straightforward. Showing in Fig. 7 are the $\bar{S}(\kappa)$ versus κ curves for different types of dislocations. It is seen that the edge and screw dislocations give the upper and lower bounds, respectively.

Example 2—Cubic materials: For cubic crystals, the elastic constants can be written as[14]

$$C_{ijkl} = C_{12}\delta_{ij}\delta_{kl} + C_{44}(\delta_{ik}\delta_{jl} + \delta_{il}\delta_{jk}) + (C_{11} - C_{12} - 2C_{44})d_{ijkl}, \tag{50}$$

where the symbol d_{ijkl} is defined by the following:

$$d_{1111} = d_{2222} = d_{3333} = 1, \quad \text{others} = 0. \tag{51}$$

Substitution of Eq. (50) into Eqs. (8)–(11) yields the line energy $K(\theta)$. Unfortunately, it does not seem possible to carry out the integral in Eq. (9) analytically. So, numerical integrations will be needed. In what follows, we will use iron (Fe) single crystal, a BCC metal, as an example to perform the numerical calculations.

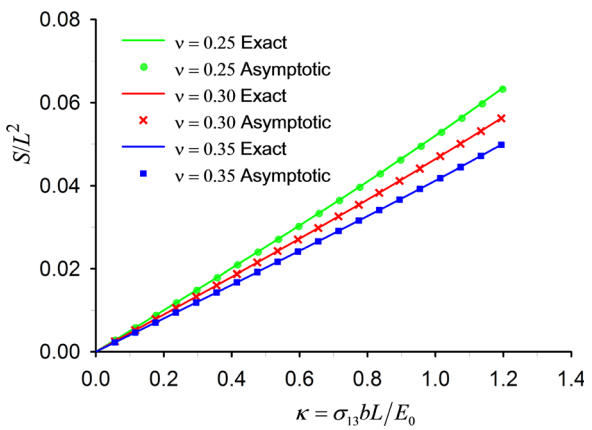

FIG. 5. S/L^2 versus κ for pure screw dislocations.

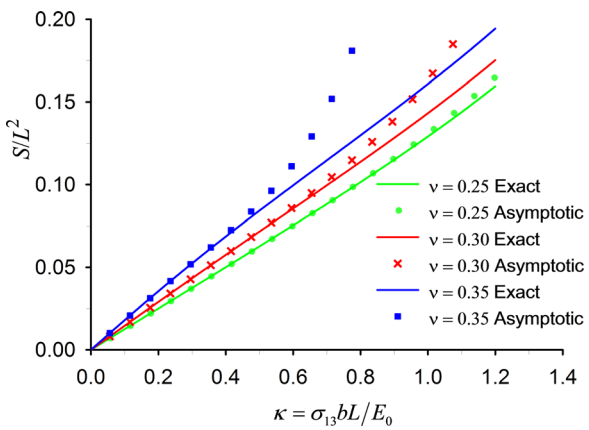

FIG. 6. S/L^2 versus κ for pure edge dislocations.

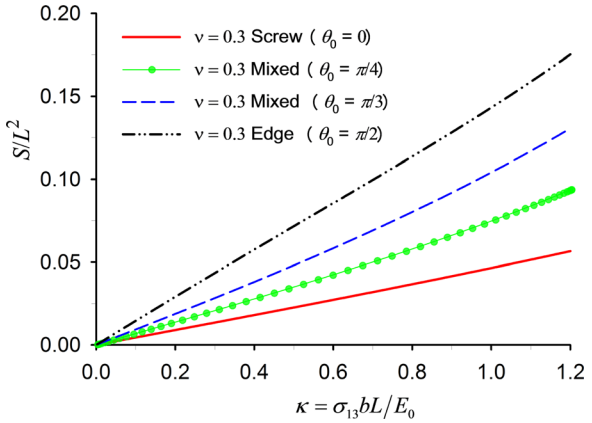

FIG. 7. S/L^2 versus κ for mixed dislocations compared with pure dislocations.

Specifically, we consider dislocations having Burgers vector in the [111] direction, and slip plane in the $(1\bar{1}0)$ plane. The elastic constants used in the numerical calculations are taken from,[15] $C_{11} = 226\,\text{GPa}$, $C_{12} = 140\,\text{GPa}$, and $C_{44} = 116\,\text{GPa}$. Carrying out the integral in Eq. (9), we found that $K(\theta)$ can be well approximated by

$$\begin{aligned} K(\theta) = {} & 0.7862 - 0.2403\cos 2\theta + 0.01611\sin 2\theta \\ & -0.03383\cos 4\theta + 0.001294\sin 4\theta \\ & -0.005534\cos 6\theta - 0.005174\sin 6\theta. \end{aligned} \tag{52}$$

The above function is plotted in Fig. 8. Although it may not be obvious from the plot, the data do show that $K(\pi/2-\theta) \neq K(\pi/2+\theta)$. This asymmetry with respect to $\theta = \pi/2$ is due to elastic anisotropy.

Making use of the expression of $K(\theta)$ given in Eq. (52), one can also plot the equilibrium contour of dislocation segments. For $L/b = 2000$, the result is shown in Fig. 9. It is seen that the bowed out shape of pure edge and screw dislocations no longer has the symmetry as seen in the isotropic case. More importantly, there are two "corner" points on the contour where the curve is not as smooth as the rest. As discussed later, these two corners can lead to some unusual behavior of the acoustic nonlinearity parameter.

By solving Eq. (22), one can obtain θ_1 and θ_2. From there, the area swept by the dislocation bowing can be

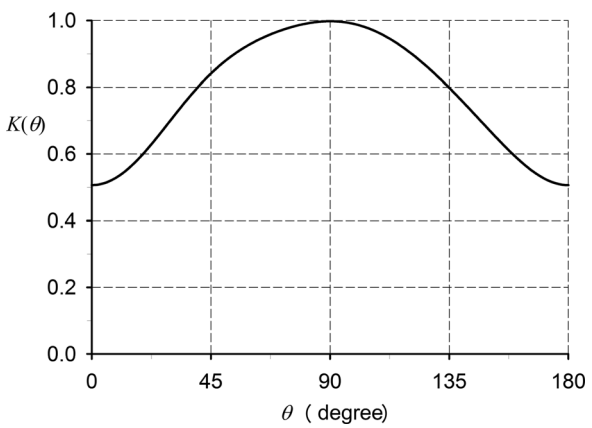

FIG. 8. $K(\theta)$ for BCC Fe.

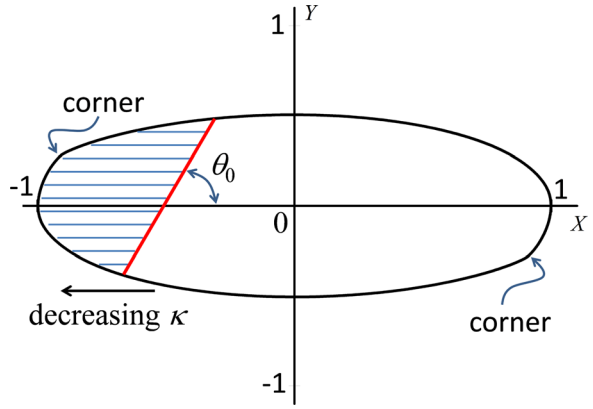

FIG. 9. Contour representing all potential equilibrium shape of a dislocation segment in BCC Fe.

obtained from Eq. (27). Showing in Fig. 10 are the corresponding $\bar{S}(\kappa)$ versus κ curves. It is seen that the pure screw dislocation remains to be the lower bound. The pure edge dislocation, however, is no longer the upper bound. At lower stress, the mixed dislocation seems to be more compliant than the pure edge dislocation. Only at higher stress, does the pure edge dislocation become more deformable. Further, the elastic anisotropy seems to have reduced the overall stiffness of the dislocation significantly in comparison with isotropic materials.

V. COMPARISON WITH MD SIMULATIONS

The foregoing modeling is based on the continuum theory of elasticity. To confirm its validity, MD simulations were performed on an edge dislocation subjected to shear stress. The MD simulation cell is a rectangular block of BCC single crystal as schematically shown in Fig. 11. For convenience, a Cartesian coordinate system (xyz) is attached to the cell representing the [111], $[1\bar{1}0]$, and the $[11\bar{2}]$ directions, respectively. The dimensions are 34.3 nm in the x-direction, 18.6 nm in the y-direction, and 42.1 nm in the z-direction, respectively. By following the approach used by Osetsky and Bacon,[16] a perfect edge dislocation is constructed along the z-direction in the center of the orthorhombic box, terminating at the cell surface. Each end of the dislocation is pinned by a nano-void.

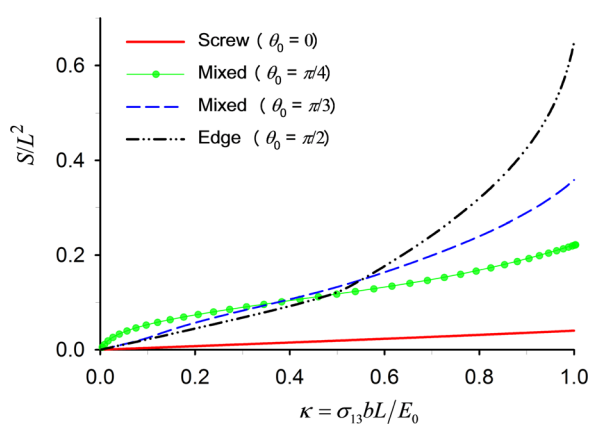

FIG. 10. S/L^2 versus κ for dislocations in BCC Fe.

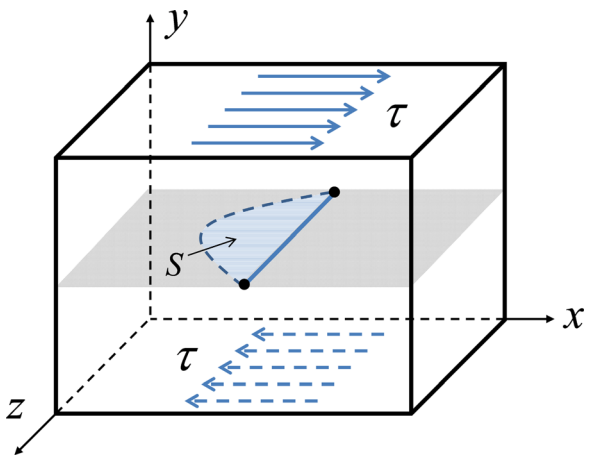

FIG. 11. BCC Fe cell with a pure edge dislocation pinned by a nano-void at each end.

During the simulation, periodic boundary conditions were prescribed in the x- and z-directions. A shear stress is applied in the x-direction on the top and bottom surfaces of the cell. The simulations were performed using the MD code LAMMPS.[17] The embedded-atom method of Finnis-Sinclair type developed by Mendelev *et al.*[18] was used. All simulations were run in the microcanonical ensemble NVE and the temperature is fixed to be 0 K, so effectively, the simulation is molecular static.

At each given stress level, the area swept by the dislocation bowing can be calculated by the locations of the atoms along the dislocation line. The results are plotted in Fig. 12. For comparison, the numerical results based on the continuum theory are also presented in Fig. 12. It is seen that the MD simulations and the continuum theory yield almost identical results at lower stress $\kappa < 0.4$. At higher stresses, the pinning points simulated by the nano-voids start to move so that data cannot be compared anymore.

VI. CRITICAL SHEAR STRESS FOR UNSTABLE DISLOCATION BOWING

It is seen from Eq. (18) that the size of the contour that represents the stable shape of the bowing dislocation decreases as κ increases. Since increasing κ means increasing the applied shear stress for a given dislocation segment length L, there must exist a critical shear stress τ_c beyond which the contour becomes so small that the two ends of the dislocation segment of a given length can no longer be on the contour simultaneously. Physically, this means that when the shear stress is at this critical value, the dislocation reaches a condition of instability. When the applied shear stress is greater than τ_c, the pinned dislocation becomes a Frank-Read source by pinching itself off the pinning points to form a Frank-Read loop.[12] In the literature, $\tau_c = 2\mu b/L$ is often used for isotropic materials. The solutions in the previous sections enable the determination of τ_c in anisotropic crystals.

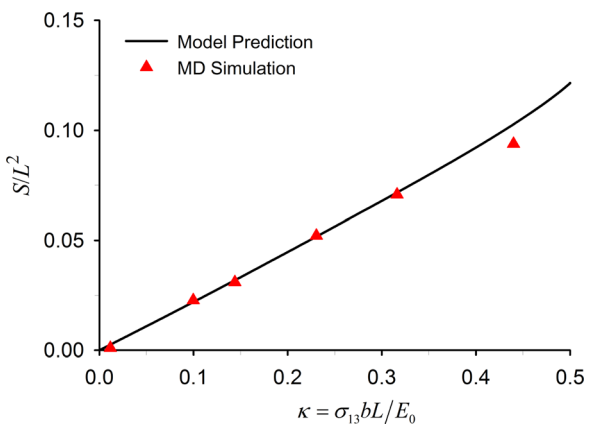

FIG. 12. S/L^2 versus κ for dislocations in BCC Fe compared with MD.

As discussed in Sec. II, $E(\theta+\pi) = E(\theta)$ and $E'(\theta+\pi) = E'(\theta)$. It thus follows from Eq. (19) that

$$X(\theta+\pi) = -X(\theta), \quad Y(\theta+\pi) = -Y(\theta). \tag{53}$$

This means that the closed contour in Fig. 3 has a central symmetry for any arbitrary anisotropic crystals. For such convex contour with central symmetry, it follows from Fig. 3 that the condition for obtaining the critical stress τ_c is when the point (AL, BL) is on the dislocation line, i.e.,

$$\frac{B}{A} = \tan\theta_0, \quad A^2 + B^2 = \frac{1}{4}. \tag{54}$$

Solving Eq. (54) leads to

$$A = \frac{\cos\theta_0}{2}, \quad B = \frac{\sin\theta_0}{2}. \tag{55}$$

Substituting the first of Eq. (55) into the first of Eq. (20) yields

$$\kappa_c = \frac{\tau_c bL}{E_0} = \frac{-2X(\theta_1)}{\cos\theta_0}, \quad \text{or}$$
$$\tau_c = \frac{-2E_0 X(\theta_1)}{bL\cos\theta_0} = \frac{-C_{44}bX(\theta_1)}{L\cos\theta_0}. \tag{56}$$

To determine θ_1, we make use of the first of Eq. (54) in Eq. (20),

$$Y(\theta_1) - X(\theta_1)\tan\theta_0 = 0, \tag{57}$$

or equivalently

$$(\sin\theta_1\tan\theta_0 + \cos\theta_1)K(\theta_1) + (\cos\theta_1\tan\theta_0 - \sin\theta_1)K'(\theta_1) = 0. \tag{58}$$

Once Eq. (58) is solved for θ_1, the critical stress can be obtained from Eq. (56).

We note that Eq. (56) was derived by Kovacs[19] for pure screw and edge dislocations. Equation (58) allows ones to solve for θ_1 for any mixed dislocations. For example, for the materials considered in previous sections, the critical stress $\kappa_c = \tau_c bL/E_0$ versus θ_0 is plotted in Fig. 13. Several observations can be made. First, elastic anisotropy seems to have reduced the critical stress significantly. Second, the critical stress is the highest when $\theta_0 = 0$, i.e., when the initial dislocation is a pure screw dislocation, and the lowest when $\theta_0 = \pm\pi/2$, i.e., when the initial dislocation is a pure edge

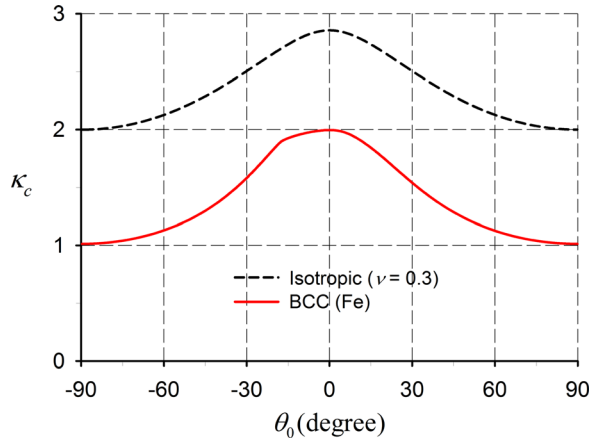

FIG. 13. κ_c versus θ_0 for isotropic and BCC Fe crystals.

dislocation. This is consistent with the findings in early sections that screw dislocations are stiffer than edge dislocations against shear stress. Finally, the κ_c versus θ_0 is not symmetric about $\theta_0 = 0$ for BCC crystals.

VII. ACOUSTIC NONLINEARITY PARAMETER

For simplicity, we will limit the discussions in this section to crystals with cubic or higher symmetry, and consider only waves traveling along one of the crystal symmetry directions, which will be designated as the $\mathbf{e}_1^c$ direction. Further, we assume that the deformation is one dimensional in the Cartesian coordinate system $\mathbf{e}_i^c$, i.e., the only non-zero stress component of the stress tensor is $\sigma_{11}^c = \sigma$, and the only non-zero strain component of the strain tensor is ε_{11}^c. For the dislocation depicted in Fig. 1 with slip direction b_i and slip plane s_i, the resolved shear stress on the slip plane can be written as $\sigma_{13} = \tau = R\sigma$, where $R = \hat{b}_1 s_1$ is the Schmidt factor that projects σ_{11}^c onto resolved shear stress in the slip direction on the slip plane. It then follows from Eq. (29) that the shear strain induced by this resolved shear written in the $\mathbf{e}_i$ system is

$$\varepsilon_{13}^{dis} = \Lambda b L \bar{S}(\kappa), \tag{59}$$

where $\kappa = R\sigma b L/E_0$. The corresponding normal strain in the $\mathbf{e}_1^c$ direction is thus given by $\Omega\varepsilon_{13}^{dis} = \Omega\Lambda b L\bar{S}(\kappa)$, where $\Omega = 2\hat{b}_1 s_1$ is the conversion factor from ε_{13}^{dis} to the normal strain in the $\mathbf{e}_1^c$ direction.

In addition to the deformation induced by dislocation bowing, the lattice itself deforms as well. The normal strain in the $\mathbf{e}_1^c$ direction due to lattice deformation is given by

$$\frac{1}{C_{1111}}\sigma - \frac{C_{111111} + 3C_{1111}}{2C_{1111}^3}\sigma^2. \tag{60}$$

The total normal strain in the $\mathbf{e}_1^c$ direction is thus the sum of the contributions from lattice deformation and dislocation bowing,

$$\varepsilon_{11}^c = \frac{1}{C_{1111}}\sigma - \frac{C_{111111} + 3C_{1111}}{2C_{1111}^3}\sigma^2 + \Omega\Lambda b L\bar{S}(\kappa). \tag{61}$$

Let us now assume that the one dimensional wave motion adds a small perturbation $\Delta\sigma$ to a solid that has a prestress σ. Let the strain perturbation corresponding to this $\Delta\sigma$ be $\Delta\varepsilon$. Thus, one may write

$$\begin{aligned}\Delta\sigma &= \frac{\partial\sigma}{\partial\varepsilon_{11}^c}\Delta\varepsilon + \frac{1}{2}\frac{\partial^2\sigma}{\partial{\varepsilon_{11}^c}^2}(\Delta\varepsilon)^2 + \cdots \\ &= \left(\frac{\partial\varepsilon_{11}^c}{\partial\sigma}\right)^{-1}\Delta\varepsilon - \frac{1}{2}\frac{\partial^2\varepsilon_{11}^c}{\partial\sigma^2}\left(\frac{\partial\varepsilon_{11}^c}{\partial\sigma}\right)^{-3}(\Delta\varepsilon)^2 + \cdots.\end{aligned} \tag{62}$$

By comparing Eq. (62) with Eq. (1), the total acoustic nonlinearity parameter corresponding to Eq. (62) can be written as

$$\beta = \frac{\partial^2\varepsilon_{11}^c}{\partial\sigma^2}\left(\frac{\partial\varepsilon_{11}^c}{\partial\sigma}\right)^{-2}. \tag{63}$$

Making use of Eq. (61) in Eq. (63) in conjunction with Eq. (29) leads to

$$\beta = \frac{\beta^l + 4\Omega R^2\left(\frac{C_{1111}}{C_{1212}}\right)^2\left(\frac{L}{b}\right)^3(\Lambda b^2)\bar{S}''(\kappa)}{\left(1 + \beta^l\left(\frac{C_{1111}}{C_{1212}}\right)^{-1}\left(\frac{L}{b}\right)^{-1}\frac{\kappa}{2} + 2\Omega R\frac{C_{1111}}{C_{1212}}\left(\frac{L}{b}\right)^2(\Lambda b^2)\bar{S}'(\kappa)\right)^2}, \tag{64}$$

where $\bar{S}'(\kappa)$ and $\bar{S}''(\kappa)$ are the first and second derivatives of $\bar{S}(\kappa)$ with respect to κ, and

$$\beta^l = -3 - \frac{C_{111111}}{C_{1111}}, \tag{65}$$

is the well-known acoustic nonlinearity parameter due to elastic lattice anharmonicity.[6] In the above, all the derivatives should be evaluated at the initial stress σ. In the limit of $\sigma \to 0$, one has

$$\lim_{\sigma\to 0}\beta = \frac{\beta^l + 4\Omega R^2\left(\frac{C_{1111}}{C_{1212}}\right)^2\left(\frac{L}{b}\right)^3(\Lambda b^2)\bar{S}''(0)}{\left(1 + 2\Omega R\frac{C_{1111}}{C_{1212}}\left(\frac{L}{b}\right)^2(\Lambda b^2)\bar{S}'(0)\right)^2}. \tag{66}$$

This represents the intrinsic acoustic nonlinearity parameter in an unstressed crystalline solid with dislocations.

It is seen from Eqs. (64) and (66) that, unless certain assumptions are made, contributions to the overall acoustic nonlinearity parameter are coupled between the lattice anharmonicity and dislocation bowing. In many cases of practical interest, $L/b \gg 1$, but $(L/b)^2(\Lambda b^2) \ll 1$. Under these assumptions, Eq. (64) can be written as

$$\beta = \beta^l + \beta^d, \tag{67}$$

where

$$\beta^d = 4\Omega R^2 \Lambda b^2 \left(\frac{C_{1111}}{C_{1212}}\right)^2 \left(\frac{L}{b}\right)^3 \bar{S}''(\kappa). \tag{68}$$

If one further assumes that the material is isotropic and the dislocation line tension is a constant, then[20]

$$C_{1111} = \lambda + 2\mu, \quad C_{111111} = 2l + 4m, \quad \bar{S}(\kappa) = \frac{\kappa}{3} + \frac{\kappa^3}{10}, \tag{69}$$

where l and m are two of the three Murnaghan coefficients of the isotropic elastic solid.

Making use of Eq. (69) in Eq. (67) leads to

$$\beta^l = -3 - \frac{2l + 4m}{\lambda + 2\mu}, \quad \beta^d = \frac{24\eta^4 R^3 \Omega \Lambda b^2}{5} \left(\frac{L}{b}\right)^4 \left(\frac{\sigma}{\mu}\right), \tag{70}$$

where

$$\eta = \frac{c_L}{c_T} = \sqrt{\frac{\lambda + 2\mu}{\mu}} = \sqrt{\frac{2(1-\nu)}{1-2\nu}}.$$

The expressions in Eq. (70) were essentially derived by Hikata *et al.*[7] in the 1960s and in more details recently by Cantrell.[6]

For more general cases, Eq. (68) needs to be evaluated numerically. Shown in Figs. 14 and 15 are the values of $\beta^d/\Lambda b^2$ versus κ at different values of the Poisson's ratio for screw and edge dislocations, respectively. To be definitive, we have used $\Omega = 2R = 2/3$ in these plots. As a comparison,

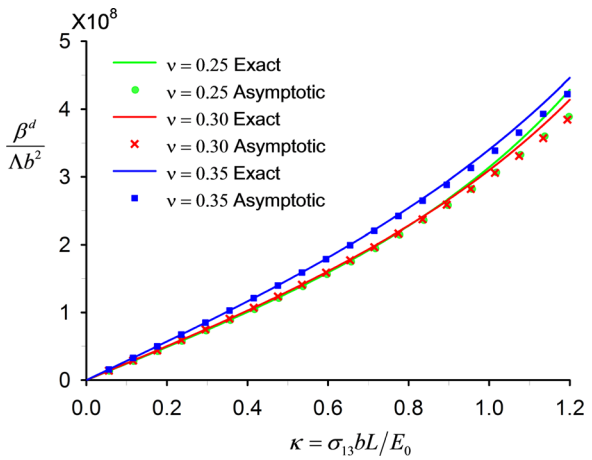

FIG. 14. $\beta^d/\Lambda b^2$ versus κ for screw dislocations.

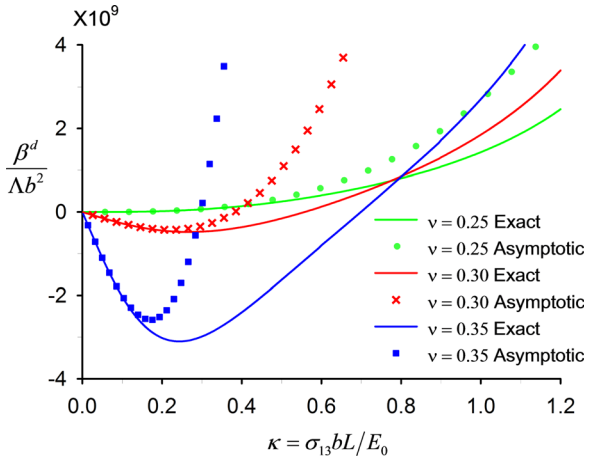

FIG. 15. $\beta^d/\Lambda b^2$ versus κ for edge dislocations.

Eq. (68) was also evaluated for these two cases by using the asymptotical solutions of the $\bar{S}(\kappa)$ given in Eqs. (43) and (48) for the screw and edge dislocations, respectively. The corresponding values are plotted in Figs. 14 and 15 using symbols. Clearly, the asymptotic solutions given in Eqs. (43) and (48) work well for the screw dislocations, but not for the edge dislocations, particularly for large values of the Poisson's ratio. More interestingly, for sufficiently large Poisson's ratio, β^d for the edge dislocation does not increase monotonically with increasing applied shear stress κ.

For mixed dislocations, the $\beta^d/\Lambda b^2$ versus κ relationship is shown in Fig. 16 for $\nu = 0.30$. Interestingly, β^d for the mixed dislocations shown in Fig. 16 does increase monotonically with increasing κ.

To investigate the effects of elastic anisotropy, the $\beta^d/\Lambda b^2$ versus κ relationship for pure and mixed dislocations in BCC Fe is plotted in Fig. 17. It is noticed that the contribution of mixed dislocations to the nonlinearity is much greater than the pure dislocations under low shear stress. More interestingly, $\beta^d/\Lambda b^2$ does not increase monotonically with increasing κ. In fact, the $\beta^d/\Lambda b^2$ versus κ curves have fairly sharp peaks around $\kappa \approx 0.1$ and $\kappa \approx 0.5$ for the cases of $\theta_0 = \pi/3$ and $\theta_0 = \pi/4$, respectively. Careful examination reveals that those peaks are due to the two corner points

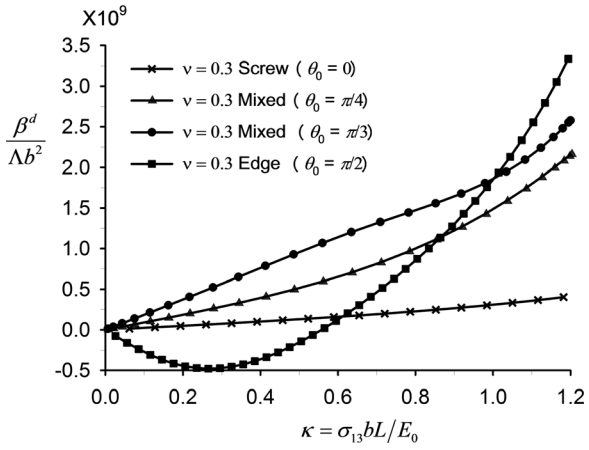

FIG. 16. $\beta^d/\Lambda b^2$ versus κ for mixed dislocations compared with pure dislocations.

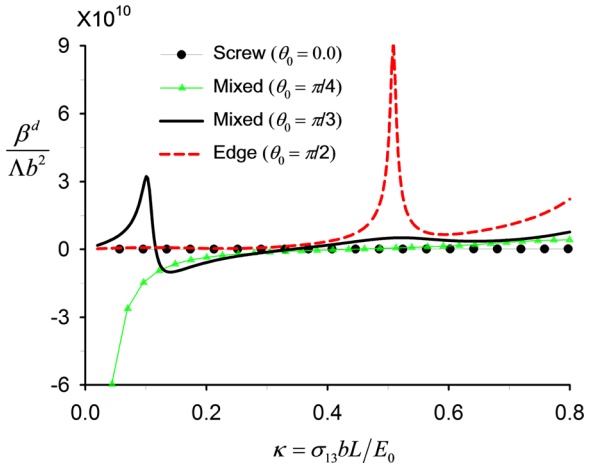

FIG. 17. $\beta^d/\Lambda b^2$ versus κ for pure dislocations in BCC Fe.

on the contour showing in Fig. 9. As illustrated in Fig. 9, the shaded area enclosed by the dislocation segment and the elliptical-like contour is $\bar{S}(\kappa)$. As κ decreases, the elliptical-like contour increases in size self-similarly. Equivalently, decreasing κ can also interpreted as shortening the dislocation length, and moving it leftwards (toward the negative X direction), while keeping the elliptical-like contour unchanged. In the latter interpretation, as the dislocation moves leftwards, the area $\bar{S}(\kappa)$ decreases. Clearly, $\bar{S}'(\kappa)$ is the rate of the area change with respect to κ, and $\bar{S}''(\kappa)$ represents the "acceleration" of the area change with respect to κ. If the elliptical-like contour is very smooth, $\bar{S}''(\kappa)$ would vary smoothly with κ. If the elliptical-like contour has a corner, then $\bar{S}''(\kappa)$ would change rapidly as the dislocation line passes through this corner. This is the cause of the peaks around $\kappa \approx 0.1$ and $\kappa \approx 0.5$ for the cases of $\theta_0 = \pi/3$ and $\theta_0 = \pi/4$, respectively.

Another noteworthy point is the value of large negative value of $\bar{S}''(\kappa)$ near $\kappa = 0$ for the case of $\theta_0 = \pi/4$. It turns out that the line tension $T(\theta_0)$ is almost zero at $\theta_0 = \pi/4$. Since $\bar{S}''(0) \propto 1/T^3(\theta_0)$, it is not surprising that $\bar{S}''(\kappa)$ near $\kappa = 0$ is large.

To close this section, we mention that in computing the acoustic nonlinearity parameter, one needs to calculate $\bar{S}''(\kappa)$. With the exception of pure dislocations in isotropic solids, $\bar{S}(\kappa)$ can be obtained only numerically. Carrying out the second derivative of a numerical solution is notoriously difficult, and the results are often inaccurate. To overcome this difficulty, we have developed a method to calculate $\bar{S}''(\kappa)$ without performing numerical derivatives. The procedure is outlined in Appendix B.

VIII. LENGTH DEPENDENCE OF β

In using nonlinear ultrasonic method to nondestructively evaluate dislocation microstructure, it is of great interest to understand the dependence of β on the dislocation microstructure such as dislocation density and segment length. To this end, let us consider Eq. (68). It is easy to see that β^d increase linearly with the dislocation density Λ. However, the dependence of β^d on the dislocation segment length L is more complicated. Note that $\kappa = \tau bL/E_0$, i.e., κ is proportional to L. Therefore, it follows from Eq. (68) that

$$h(a) = \frac{\beta^d(aL)}{\beta^d(L)} = a^3 \frac{\bar{S}''(a\kappa)}{\bar{S}''(\kappa)}. \tag{71}$$

Since $\bar{S}(\kappa)$ can be calculated from Eq. (28) for any value of κ, independent of L, the ratio $h(a) = \bar{S}''(a\kappa)/\bar{S}''(\kappa)$ is a known function of a if the orientation of the dislocation line in the crystal and its associated Burgers vector is known. Therefore, $\beta^d(L)$ can be measured for length L, then $\beta^d(aL)$ can be computed from Eq. (71) for dislocation length aL. More importantly, if both $\beta^d(L)$ and $\beta^d(aL)$ are known from experimental measurements, then Eq. (71) provides an equation from which a can be solved. This gives a means to experimentally monitor the change in dislocation length by measuring the change in the acoustic nonlinearity parameter.

To illustrate the above, we consider a special case where we assume that the solid is isotropic containing pure dislocations. It then follows from Eq. (43) for screw dislocations and Eq. (48) for edge dislocations that

$$\bar{S} \approx s_1\kappa + s_3\kappa^3. \tag{72}$$

Thus, $\bar{S}''(\kappa) = 6s_3\kappa$. It then follows from Eq. (71) that

$$h(a) = \frac{\beta^d(aL)}{\beta^d(L)} = a^3 \frac{\bar{S}''(a\kappa)}{\bar{S}''(\kappa)} = a^4. \tag{73}$$

In other words, if both $\beta^d(L)$ and $\beta^d(aL)$ are measured experimentally, the constant a can be solved immediately from Eq. (73).

For more general cases, $\bar{S}''(\kappa)$ needs to be calculated numerically. Therefore, Eq. (71) will need to be solved numerically to obtain a for a given pair of $\beta^d(L)$ and $\beta^d(aL)$. In the example below, we consider a BCC Fe crystal under the applied stress $\kappa = 0.05$. Instead of conducting actual ultrasonic measurements, we will generate a set of synthetic experimental data for $\beta^d(L)$ and $\beta^d(aL)$ by computing them from Eq. (68). This set of synthetic experimental data for $h(a) = \beta^d(aL)/\beta^d(L)$ is plotted for various values of a in Fig. 18 using solid lines. Now that $h(a) = \beta^d(aL)/\beta^d(L)$ is known from the "experiments," the corresponding a can be

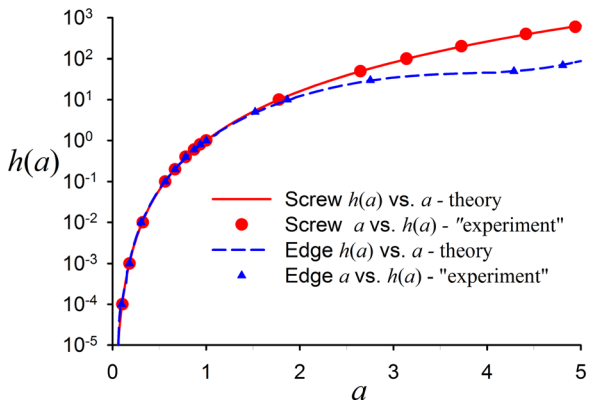

FIG. 18. Relationship between $h(a) = \beta^d(aL)/\beta^d(L)$ and a. Solid lines are $h(a)$ versus a, and symbols are a versus $h(a)$.

solved from Eq. (71) for each data point $h(a) = \beta^d(aL)/\beta^d(L)$. The a versus $h(a)$ relationship so obtained is plotted in Fig. 18 using the symbols. It is seen that the dislocation length a obtained from the experimental data $h(a) = \beta^d(aL)/\beta^d(L)$ by using Eq. (71) matches the actual a very well. Another interesting observation is that $h(a)$ remains relatively unchanged for edge dislocation, but increases significantly for screw dislocations. This means that β^d is much more sensitive to the dislocation length for screw dislocations than for edge dislocations.

IX. SUMMARY AND CONCLUSIONS

In this paper, we presented a solution to the orientation-dependent dislocation line energy in anisotropic single crystals. Making use of this solution, a method was developed to calculate the shear strain due to dislocation bowing. Ultimately, the solution to the dislocation-induced shear strain was used to calculate the acoustic nonlinearity parameter in anisotropic crystals. These solutions are new to the literature, and they reduce to known results in the literature for pure dislocations in isotropic materials. These solutions were also compared with MD simulations. Good agreements were observed.

Major conclusions from these solutions include (i) elastic anisotropy can significantly change the nonlinear behavior of dislocations including "corners" in the bowed dislocation line, much reduced critical stress for instability, sharp peaks in the β versus applied shear relationship, etc., (ii) mixed dislocations may have distinct behavior that is not bounded by pure edge and screw dislocations, and (iii) asymptotic solutions of the acoustic nonlinearity parameter in terms of power series (as high as 5th order) may not be valid, even for pure dislocations in isotropic solids. The solution to the acoustic nonlinearity parameter also enables us to develop a scaling relationship between the acoustic nonlinearity parameter and the dislocation length, from which the average dislocation length can be estimated nondestructively by conducting ultrasonic measurements.

As a by-product, the solution was also obtained for the critical shear stress that marks the onset of generating Frank-Read loops from pinned dislocations. It shows explicitly how the critical stress depends on the dislocation length, orientation, and elastic constants of the crystal. Numerical results indicate that elastic anisotropy may reduce the critical stress significantly.

In addition, an efficient method was developed to evaluate the derivatives of the dislocation-induced strain (or area swept by dislocation bowing) with respect to the applied shear stress without performing numerical derivatives. This is critical in computing the acoustic nonlinearity parameter, because it involves the second derivative of the area swept by the dislocation bowing, and the area can only be obtained numerically in discrete form.

ACKNOWLEDGMENTS

The authors greatly appreciate the discussions with Professor David Barnett on the coordinate-free nature of the Barnett-Lothe tensors, which motivated and formed the basis for this work. The work was supported in part by the U.S. Department of Energy's Nuclear Energy University Program through Standard Research Contract Nos. 00126931 and 00127346.

APPENDIX A: EXPLICIT EXPRESSION OF $f(\theta_1, \theta_2)$

$$
\begin{aligned}
\bar{S}(\theta_1,\theta_2) = {} & 24(\nu-2)\nu\sin 2\theta_0 + \nu^2\sin[2(\theta_0-3\theta_1)] \\
& +8\nu\sin[2(\theta_0-2\theta_1)] - 4\nu^2\sin[2(\theta_0-2\theta_1)] + 16\sin[2(\theta_0-\theta_1)] \\
& -16\nu\sin[2(\theta_0-\theta_1)] - 2\nu^2\sin[2(\theta_0-\theta_1)] + 16\nu\sin[2\theta_1] \\
& -8\nu^2\sin[2\theta_1] - 3\nu^2\sin[4\theta_1] + 9\nu^2\sin[2(\theta_0+\theta_1)] \\
& +\nu^2\sin[2(\theta_0-3\theta_2)] - 8\nu\sin[2\theta_0-\theta_1-3\theta_2] + 4\nu^2\sin[2\theta_0-\theta_1-3\theta_2] \\
& -8\nu\sin[\theta_1-3\theta_2] + 4\nu^2\sin[\theta_1-3\theta_2] + 6\nu^2\sin[2\theta_0+\theta_1-3\theta_2] \\
& +8\nu\sin[2(\theta_0-2\theta_2)] - 4\nu^2\sin[2(\theta_0-2\theta_2)] + 16\sin[2(\theta_0-\theta_2)] \\
& -16\nu\sin[2(\theta_0-\theta_2)] - 2\nu^2\sin[2(\theta_0-\theta_2)] - 8\nu\sin[2\theta_0-3\theta_1-\theta_2] \\
& +4\nu^2\sin[2\theta_0-3\theta_1-\theta_2] - 32\sin[2\theta_0-\theta_1-\theta_2] + 32\nu\sin[2\theta_0-\theta_1-\theta_2] \\
& -8\nu^2\sin[2\theta_0-\theta_1-\theta_2] - 32\sin[\theta_1-\theta_2] + 32\nu\sin[\theta_1-\theta_2] \\
& +10\nu^2\sin[\theta_1-\theta_2] - 2\nu^2\sin[3(\theta_1-\theta_2)] + 24\nu\sin[2\theta_0+\theta_1-\theta_2] \\
& -12\nu^2\sin[2\theta_0+\theta_1-\theta_2] - 8\nu\sin[3\theta_1-\theta_2] + 4\nu^2\sin[3\theta_1-\theta_2] \\
& -16\nu\sin[2\theta_2] + 8\nu^2\sin[2\theta_2] + 3\nu^2\sin[4\theta_2] + 9\nu^2\sin[2(\theta_0+\theta_2)] \\
& +6\nu^2\sin[2\theta_0-3\theta_1+\theta_2] + 24\nu\sin[2\theta_0-\theta_1+\theta_2] - 12\nu^2\sin[2\theta_0-\theta_1+\theta_2] \\
& -18\nu^2\sin[2\theta_0+\theta_1+\theta_2] + 6\nu^2\sin[3\theta_1+\theta_2] - 6\nu^2\sin[\theta_1+3\theta_2] \\
& -2\nu^2\sin[2\theta_0-3(\theta_1+\theta_2)] + 32\theta_1 - 32\nu\theta_1 - 4\nu^2\theta_1 - 32\theta_2 + 32\nu\theta_2 + 4\nu^2\theta_2. \qquad \text{(A1)}
\end{aligned}
$$

APPENDIX B: NUMERICAL PROCEDURE TO CALCULATE $\bar{S}''(\kappa)$

For convenience, we write

$$\bar{S}(\kappa) = \kappa^{-2}\int_{\theta_1}^{\theta_2} f(\theta)d\theta - \kappa^{-1}g(\theta_1), \tag{B1}$$

where

$$f(\theta) = -g(\theta)\frac{\partial g'(\theta)}{\partial \theta_0}, \quad g(\theta) = -X(\theta)\sin\theta_0 + Y(\theta)\cos\theta_0. \tag{B2}$$

Thus,

$$\begin{aligned}\bar{S}'(\kappa) =& -2\kappa^{-3}\int_{\theta_1}^{\theta_2} f(\theta)d\theta + \kappa^{-2}g(\theta_1)\\ &+\kappa^{-2}\left[f(\theta_2)\frac{\partial\theta_2}{\partial\kappa} - f(\theta_1)\frac{\partial\theta_1}{\partial\kappa}\right] - \kappa^{-1}g'(\theta_1)\frac{\partial\theta_1}{\partial\kappa},\end{aligned} \tag{B3}$$

$$\begin{aligned}\bar{S}''(\kappa) =& 6\kappa^{-4}\int_{\theta_1}^{\theta_2} f(\theta)d\theta - 2\kappa^{-3}g(\theta_1) + 2\kappa^{-2}g'(\theta_1)\frac{\partial\theta_1}{\partial\kappa}\\ &+4\kappa^{-3}\left[f(\theta_2)\frac{\partial\theta_2}{\partial\kappa} - f(\theta_1)\frac{\partial\theta_1}{\partial\kappa}\right]\\ &+\kappa^{-2}\left[f'(\theta_2)\left(\frac{\partial\theta_2}{\partial\kappa}\right)^2 + f(\theta_2)\frac{\partial^2\theta_2}{\partial\kappa^2}\right.\\ &\left.-f'(\theta_1)\left(\frac{\partial\theta_1}{\partial\kappa}\right)^2 - f(\theta_1)\frac{\partial^2\theta_1}{\partial\kappa^2}\right]\\ &-\kappa^{-1}\left[g''(\theta_1)\left(\frac{\partial\theta_1}{\partial\kappa}\right)^2 + g'(\theta_1)\frac{\partial^2\theta_1}{\partial\kappa^2}\right].\end{aligned} \tag{B4}$$

It can be computed that

$$g(\theta) = K(\theta)\cos(\theta-\theta_0) - K'(\theta)\sin(\theta-\theta_0), \tag{B5}$$

$$\begin{aligned}g'(\theta) &= -T(\theta)\sin(\theta-\theta_0),\\ g''(\theta) &= -T(\theta)\cos(\theta-\theta_0) - T'(\theta)\sin(\theta-\theta_0),\end{aligned} \tag{B6}$$

$$\begin{aligned}f'(\theta) =& \frac{1}{2}\sin[2(\theta-\theta_0)](T(\theta))^2\\ &+(T(\theta)\sin(\theta-\theta_0) - T'(\theta)\cos(\theta-\theta_0))\\ &\times(K(\theta)\cos(\theta-\theta_0) - K'(\theta)\sin(\theta-\theta_0)),\end{aligned} \tag{B7}$$

where $T(\theta) = K(\theta) + K''(\theta)$ is the dislocation line tension.

Note that θ_1 and θ_2 satisfy Eq. (22). Thus,

$$\begin{aligned}X'(\theta_2)\frac{\partial\theta_2}{\partial\kappa} - X'(\theta_1)\frac{\partial\theta_1}{\partial\kappa} &= \cos\theta_0,\\ Y'(\theta_2)\frac{\partial\theta_2}{\partial\kappa} - Y'(\theta_1)\frac{\partial\theta_1}{\partial\kappa} &= \sin\theta_0.\end{aligned} \tag{B8}$$

Solving these two equations, one arrives at

$$\begin{bmatrix}\frac{\partial\theta_1}{\partial\kappa}\\ \frac{\partial\theta_2}{\partial\kappa}\end{bmatrix} = \mathbf{A}^{-1}(\kappa)\begin{bmatrix}\cos\theta_0\\ \sin\theta_0\end{bmatrix} = \frac{1}{\sin(\theta_2-\theta_1)}\begin{bmatrix}\frac{\sin(\theta_2-\theta_0)}{T(\theta_1)}\\ \frac{\sin(\theta_1-\theta_0)}{T(\theta_2)}\end{bmatrix}, \tag{B9}$$

$$\begin{bmatrix}\frac{\partial^2\theta_1}{\partial\kappa^2}\\ \frac{\partial^2\theta_2}{\partial\kappa^2}\end{bmatrix} = -\mathbf{A}^{-1}(\kappa)\frac{\partial\mathbf{A}(\kappa)}{\partial\kappa}\mathbf{A}^{-1}(\kappa)\begin{bmatrix}\cos\theta_0\\ \sin\theta_0\end{bmatrix}, \tag{B10}$$

where

$$\mathbf{A}(\kappa) = \begin{bmatrix}-X'(\theta_1) & X'(\theta_2)\\ -Y'(\theta_1) & Y'(\theta_2)\end{bmatrix} = \begin{bmatrix}T(\theta_1)\cos\theta_1 & -T(\theta_2)\cos\theta_2\\ T(\theta_1)\sin\theta_1 & -T(\theta_2)\sin\theta_2\end{bmatrix}, \tag{B11}$$

$$\mathbf{A}^{-1}(\kappa) = \frac{1}{\sin(\theta_2-\theta_1)}\begin{bmatrix}\frac{\sin\theta_2}{T(\theta_1)} & -\frac{\cos\theta_2}{T(\theta_1)}\\ \frac{\sin\theta_1}{T(\theta_2)} & -\frac{\cos\theta_1}{T(\theta_2)}\end{bmatrix}, \tag{B12}$$

$$\frac{\partial\mathbf{A}(\kappa)}{\partial\kappa} = \begin{bmatrix}-X''(\theta_1)\frac{\partial\theta_1}{\partial\kappa} & X''(\theta_2)\frac{\partial\theta_2}{\partial\kappa}\\ -Y''(\theta_1)\frac{\partial\theta_1}{\partial\kappa} & Y''(\theta_2)\frac{\partial\theta_2}{\partial\kappa}\end{bmatrix}, \tag{B13}$$

where

$$X'(\theta) = -T(\theta)\cos(\theta), \quad Y'(\theta) = -T(\theta)\sin(\theta), \tag{B14}$$

$$\begin{aligned}X''(\theta) &= T(\theta)\sin\theta - T'(\theta)\cos(\theta),\\ Y''(\theta) &= -T(\theta)\cos\theta - T'(\theta)\sin\theta.\end{aligned} \tag{B15}$$

It is seen from the above that $\bar{S}''(\kappa)$ can be computed without performing numerical differentiation if $K(\theta)$, $K''(\theta)$, and $K^{(3)}(\theta)$ can be evaluated without performing numerical differentiation. To this end, one only needs to evaluate the derivatives of $\mathbf{L}(\theta)$, see Eq. (8). According to Eq. (9),

$$\begin{aligned}\mathbf{L}'(\theta) =& -\frac{1}{\pi}\int_0^\pi(\mathbf{R}'\mathbf{T}^{-1}\mathbf{R}^T - \mathbf{R}\mathbf{T}^{-1}\mathbf{T}'\mathbf{T}^{-1}\mathbf{R}^T\\ &+\mathbf{R}\mathbf{T}^{-1}\mathbf{R}'^T - \mathbf{Q}')d\omega,\end{aligned} \tag{B16}$$

$$\begin{aligned}\mathbf{L}''(\theta) =& -\frac{1}{\pi}\int_0^\pi(\mathbf{R}''\mathbf{T}^{-1}\mathbf{R}^T - 2\mathbf{R}'\mathbf{T}^{-1}\mathbf{T}'\mathbf{T}^{-1}\mathbf{R}^T\\ &+2\mathbf{R}'\mathbf{T}^{-1}\mathbf{R}'^T + \mathbf{R}\mathbf{T}^{-1}\mathbf{R}''^T)d\omega\\ &+\frac{1}{\pi}\int_0^\pi(-2\mathbf{R}\mathbf{T}^{-1}\mathbf{T}'\mathbf{T}^{-1}\mathbf{T}'\mathbf{T}^{-1}\mathbf{R}^T\\ &+\mathbf{R}\mathbf{T}^{-1}\mathbf{T}''\mathbf{T}^{-1}\mathbf{R}^T + 2\mathbf{R}\mathbf{T}^{-1}\mathbf{T}'\mathbf{T}^{-1}\mathbf{R}'^T)d\omega\\ &\times\frac{1}{\pi}\int_0^\pi\mathbf{Q}''d\omega.\end{aligned} \tag{B17}$$

Clearly, $\mathbf{L}^{(3)}(\theta)$ can be calculated in a straightforward fashion, albeit the expression is long. In order to evaluate these derivatives, the derivatives of the Barnet-Lothe tensors are needed. This requires the derivatives of **m** and **n** with respect to θ. They can be computed from their definitions given in Eqs. (13) and (14),

$$\begin{aligned}\mathbf{m}' &= \cos\omega(-\sin\theta\mathbf{s}\times\hat{\mathbf{b}} - \cos\theta\hat{\mathbf{b}}),\\ \mathbf{n}' &= -\sin\omega(-\sin\theta\mathbf{s}\times\hat{\mathbf{b}} - \cos\theta\hat{\mathbf{b}}),\end{aligned} \tag{B18}$$

$$\begin{aligned}\mathbf{m}'' &= -\cos\omega(\cos\theta\mathbf{s}\times\hat{\mathbf{b}} - \sin\theta\hat{\mathbf{b}}),\\ \mathbf{n}'' &= \sin\omega(\cos\theta\mathbf{s}\times\hat{\mathbf{b}} - \sin\theta\hat{\mathbf{b}}),\end{aligned} \tag{B19}$$

$$\mathbf{m}^{(3)} = -\mathbf{m}', \quad \mathbf{n}^{(3)} = -\mathbf{n}'. \tag{B20}$$

Consequently,

$$\begin{aligned}R'_{ij} &= C_{pijq}(m'_p n_q + m_p n'_q),\\ R''_{ij} &= C_{pijq}(m''_p n_q + 2m'_p n'_q + m_p n''_q),\end{aligned} \tag{B21}$$

$$\begin{aligned}R^{(3)}_{ij} &= C_{pijq}(-m'_p m_q + 3m''_p m'_q + 3m'_p m''_q - m_p m'_q)\\ &= C_{pijq}(3m''_p n'_q + 3m'_p n''_q) - R'_{ij},\end{aligned} \tag{B22}$$

$$\begin{aligned}Q'_{ij} &= C_{pijq}(m'_p m_q + m_p m'_q),\\ Q''_{ij} &= C_{pijq}(m''_p m_q + 2m'_p m'_q + m_p m''_q),\end{aligned} \tag{B23}$$

$$\begin{aligned}Q^{(3)}_{ij} &= C_{pijq}(-m'_p m_q + 3m''_p m'_q + 3m'_p m''_q - m_p m'_q)\\ &= C_{pijq}(3m''_p m'_q + 3m'_p m''_q) - Q'_{ij}.\end{aligned} \tag{B24}$$

Similar expressions can be obtained for T_{ij} by replacing the **m** in **Q** with **n**. From the above, one can see that $\mathbf{L}'(\theta)$, $\mathbf{L}''(\theta)$, and $\mathbf{L}^{(3)}(\theta)$, and consequently $K(\theta)$, $K''(\theta)$, and $K^{(3)}(\theta)$, can be evaluated without performing numerical differentiation.

[1]S. V. Walker, J. Y. Kim, J. M. Qu, and L. J. Jacobs, Ndt & E Int. **48**, 10–15 (2012).
[2]M. H. Liu, G. X. Tang, L. J. Jacobs, and J. M. Qu, J. Appl. Phys. **112**(2), 024908 (2012).
[3]C. Pruell, J. Y. Kim, J. M. Qu, and L. J. Jacobs, Smart Mater. Struct. **18**(3), 035003 (2009).
[4]K. H. Matlack, J. Y. Kim, L. J. Jacobs, and J. M. Qu, J. Appl. Phys. **109**(1), 014905 (2011).
[5]A. N. Norris, in *Nonlinear Acoustics*, edited by M. F. Hamilton and D. T. Blackstock (Academic Press, San Diego, 1997), pp. 263–277.
[6]J. Cantrell, in *Ultrasonic Nondestructive Evaluation*, edited by T. Kundu (CRC Press, New York, 2004), pp. 363–433.
[7]A. Hikata, B. B. Chick, and C. Elbaum, J. Appl. Phys. **36**(1), 229–236 (1965).
[8]W. D. Cash and W. Cai, J. Appl. Phys. **109**(1), 014915 (2011).
[9]D. Bacon, D. M. Barnett, and R. O. Scattergood, Prog. Mater. Sci. **23**, 51–262 (1980).
[10]J. Qu and Q. Li, J. Elast. **26**(2), 169–195 (1991).
[11]T. C. T. Ting, *Anisotropic Elasticity—Theory and Applications* (Oxford Science Publications, 1996).
[12]G. Dewit and J. S. Koehler, Phys. Rev. **116**(5), 1113–1120 (1959).
[13]D. M. Barnett and D. L. Yaney, Scr. Metall. **20**, 787–788 (1986).
[14]J. Qu and M. Cherkaoui, *Fundamentals of Micromechanics of Solids* (John Wiley & Sons, Inc., Hoboken, NJ, 2006).
[15]D. R. Lide, *CRC Handbook of Chemistry and Physics* (CRC Press, 2012).
[16]Y. N. Osetsky and D. J. Bacon, Modell. Simul. Mater. Sci. Eng. **11**(4), 427–446 (2003).
[17]S. J. Plimpton, J. Comput. Phys. **117**, 1 (1995), see http://lammps.sandia.gov.
[18]M. Mendelev, S. Han, D. Srolovitz, G. Ackland, D. Sun, and M. Asta, Philos. Mag. **83**(35), 3977–3994 (2003).
[19]I. Kovacs, Phys. Status Solidi **3**(1), 140–144 (1963).
[20]J. Cantrell, in *Ultrasonic Nondestructive Evaluation*, edited by T. Kundu (CRC Press, New York, 2004), pp. 363.